Applied Surface Science 613 (2023) 155918

Contents lists available at ScienceDirect

Applied Surface Science

journal homepage: www.elsevier.com/locate/apsusc

Full Length Article

Electronically ordered ultrathin Cr_2O_3 on Pt(1 1 1) in presence of a multidomain graphene intralayer

Sara Fiori [a,*], Deepak Dagur [a,b], Michele Capra [c], Andrea Picone [c], Alberto Brambilla [c], Piero Torelli [a], Giancarlo Panaccione [a], Giovanni Vinai [a,*]

[a] Istituto Officina dei Materiali (IOM)-CNR, Area Science Park, S.S. 14 km 163.5, Trieste 34149, Italy
[b] Department of Physics, University of Trieste, Via A. Valerio 2, Trieste 34127, Italy
[c] Department of Physics, Politecnico di Milano, Milano 20133, Italy

ARTICLE INFO

Keywords:
2D oxide
Interfaces
Electronic properties
Cr_2O_3
Graphene

ABSTRACT

In the last decade, reducing the dimensionality of materials to few atomic layers thickness has allowed exploring new physical properties and functionalities otherwise absent out of the two dimensional limit. In this regime, interfaces and interlayers play a crucial role. Here, we investigate their influence on the electronic properties and structural quality of ultrathin Cr_2O_3 on Pt(1 1 1), in presence of a multidomain graphene intralayer. Specifically, by combining Low-Energy Electron Diffraction, X-ray Photoelectron Spectroscopy and X-ray Absorption Spectroscopy, we confirm the growth of high-quality ultrathin Cr_2O_3 on bare Pt, with sharp surface reconstructions, proper stoichiometry and good electronic quality. Once a multidomain graphene intralayer is included at the metal/oxide interface, the Cr_2O_3 maintained its correct stoichiometry and a comparable electronic quality, even at the very first monolayers, despite the partially lost of the morphological long-range order. These results show how ultrathin Cr_2O_3 films are slightly affected by the interfacial epitaxial quality from the electronic point of view, making them potential candidates for graphene-integrated heterostructures.

1. Introduction

The first isolation of graphene (Gr) [1] in 2004 opened the way to the investigation of a plethora of low-dimensional materials, whose properties in the 2D limit were often deviating from their respective bulk ones. The investigation of 2D systems became a challenge involving several fields of research [2–5] and stimulating the design of heterostructures aimed to realize new technological devices [6,7].

In this framework, interfaces are expected to play a key role, especially in the case of ferromagnetic- (FM) and/or antiferromagnetic- (AF) based spintronic systems [8,9], since long-range order is generally required to establish controlled magnetic properties. In particular, in the case of 2D AF oxides the strong correlation between structural and magnetic properties makes the requirement of long-range order even stronger [10,11]. For this reason, the control of the epitaxial growth and the evaluation of the electronic properties are mandatory starting requirements for their further exploitations in potential innovative technological applications.

Recently, 2D AF oxide nanostructures interfaced with metallic substrates have attracted great attention [12–14], since this combination allows exploiting the conductive substrate to determine and sometimes manipulate the electronic properties of the interfacial 2D oxide. In this context, chromium oxide (Cr_2O_3) represents a particularly intriguing case due to the variety of its properties. Being active in the catalytic dehydrogenation of alkanes [15], it is widely investigated for catalytic oxidation reactions, particularly in relation to the elimination of environmentally-unfriendly compounds [16]. Together with this, it is a magnetoelectric material with antiferromagnetic order, with a Néel temperature of 307 K in the bulk form [17–19], making it a widely investigated material also in relation to the rapidly developing field of antiferromagnetic spintronics [20]. Once in thin film form, structural and interfacial properties modify its magnetic response, with a general reduction of its Néel temperature [21,22]. Cr_2O_3 thin layers are usually grown on metal supports (for instance bare Pt and Cu) by evaporating metallic Cr in oxygen atmosphere, thus resulting in morphologically well-ordered films [23,24]. Recently, a high-quality Cr_2O_3 ultrathin film was achieved on an epitaxial Gr layer grown on a ferromagnetic Ni(1 1 1) single crystal, thus demonstrating the layer-by-layer growth of

* Corresponding authors.
E-mail addresses: fiori@iom.cnr.it (S. Fiori), vinai@iom.cnr.it (G. Vinai).

https://doi.org/10.1016/j.apsusc.2022.155918
Received 27 September 2022; Received in revised form 17 November 2022; Accepted 27 November 2022
Available online 1 December 2022

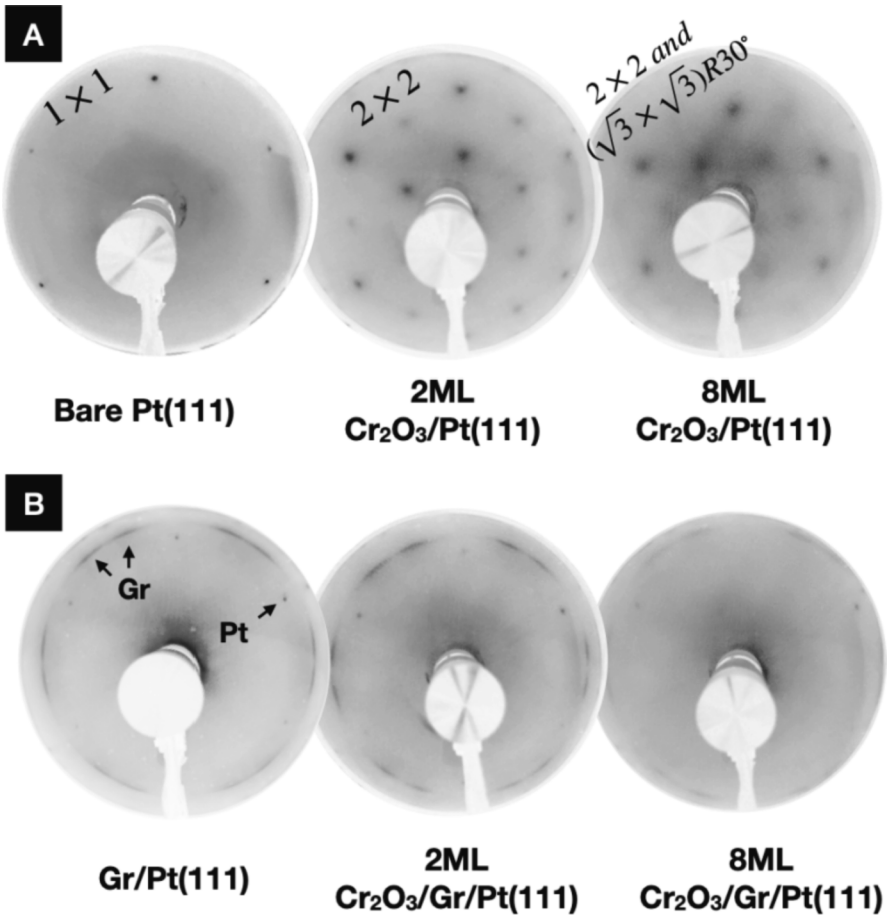

Fig. 1. The evolution of the LEED patterns is shown for the clean substrates and for the investigated Cr_2O_3 incremental growths in the case of (A) Cr_2O_3/Pt(1 1 1) and (B) Cr_2O_3/Gr/Pt(1 1 1). In the case of Cr_2O_3/Pt(1 1 1), after 2 MLs of Cr oxide a (2×2) reconstruction is found, which evolves in an additional $(\sqrt{3}\times\sqrt{3})R30^\circ$ after an incremental deposition up to 8 MLs of Cr_2O_3. On the other hand, in the case of Cr_2O_3/Gr/Pt(1 1 1), no new reconstructions are found. Electron energy: (A) 70 eV, 100 eV, 110 eV, bare Pt, 2 MLs and 8 MLs Cr_2O_3/Pt (1 1 1) respectively; (B) 70 eV, 75 eV, 65 eV, Gr/Pt, 2 MLs and 8 MLs Cr_2O_3/Gr/Pt(1 1 1) respectively.

chromium oxide on Gr/Ni [25]. The electronic structure of the Cr_2O_3/Gr interface was then investigated by using the first-principles density functional theory (DFT) calculations and angle-resolved photoemission spectroscopy (ARPES) [26]. ARPES results show the existence of predicted mid-gap interfacial states, demonstrating that the spin direction of mid-gap states can be manipulated by the substrate magnetization direction. Therefore, the insertion of a Gr interlayer at the metal/oxide interface has a key role for possible implementations in spintronic devices, since it could act as a bottom electrode below the magnetoelectric/AF layer in an integrated graphene-based device. However, graphene properties are significantly affected by the substrate on which it is grown: when graphene grows on Ni(1 1 1) single crystal, its band structure is strongly hybridized with that of Ni [27]; on other substrates, such as Pt, graphene acts as a quasi-free standing layer [28]. This drastically different graphene behavior, due to the different interaction with the substrate, stimulates further investigations of its growth on non-FM substrates as a starting step for spintronic-oriented multilayer heterostructures.

In this context, here we present a comparative investigation on the electronic properties of ultrathin Cr_2O_3 films on Pt(1 1 1) and Gr/Pt (1 1 1) templates. By combining Low-Energy Electron Diffraction (LEED), X-ray Photoemission Spectroscopy (XPS) and X-ray Absorption Spectroscopy (XAS), we report on the growth of high-quality and stoichiometric Cr_2O_3 from the first monolayers (MLs) on bare Pt. Once the Gr intralayer is included, Cr_2O_3 films maintain their stoichiometric and electronic properties mostly unaltered, despite the growth on an inhomogeneous patchwork of rotated Gr domains. These results prove the high stability of the electronic properties of ultrathin Cr_2O_3, which do not require ideal interfaces and epitaxial growth, making it a candidate material for 2D-based integrated systems.

2. Materials and methods

Pt(1 1 1) single crystal surface was cleaned by several cycles of Ar^+ sputtering at 1.5 keV for 10–15 min and annealed at around 700 °C for 10 min.

Gr growth was performed in UHV conditions by low-pressure Chemical Vapor Deposition (LP-CVD), using Ethylene (C_2H_4) as precursor. Pt(1 1 1) crystal was kept at 650 °C while dosing C_2H_4 at a partial pressure of 2×10^{-6} mbar for 15 min, followed by an additional 10 min annealing to promote the desorption of not reacted molecules stuck at the surface.

Cr_2O_3 was grown on bare Pt(1 1 1) and on Gr/Pt(1 1 1) by evaporating, via electron beam deposition, metallic Cr in a molecular oxygen partial pressure of 1×10^{-6} mbar, while keeping the substrates at around 300 °C. The average deposition rate was measured by a quartz microbalance and kept at 0.3 Å/min (the ML thickness was assumed to be ~2 Å [25]). After the deposition, the sample was kept at 300 °C for few more minutes to promote the reorganization of Cr_2O_3 on top of the sample surface [25]. All investigated thicknesses have been obtained via incremental growths.

LEED, Scanning Tunneling Microscopy (STM) and XPS characterizations were carried out at the NFFA facility of CNR-IOM in Trieste (Italy) to assess the quality and homogeneity of the samples before Cr_2O_3 deposition on bare Pt and Gr/Pt. LEED and STM measurements were carried out in a UHV chamber (base pressure of ~ 4×10^{-10} mbar). STM topographic images were acquired in constant-current mode and analyzed with the Gwyddion software package [29]. After deposition, LEED patterns were acquired to check the Cr_2O_3 growth quality and the long-range order of the samples surface. XPS and XAS measurements were carried out at APE-HE beamline of NFFA at the Elettra synchrotron

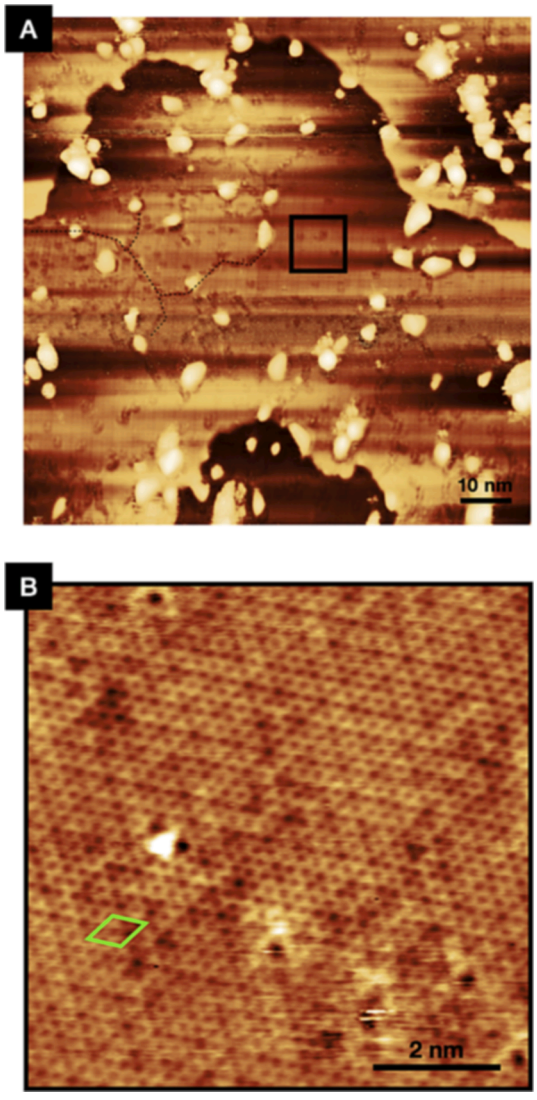

Fig. 2. (A) Large scale STM topographical image of Gr/Pt(1 1 1). Black dashed lines indicate the grain boundaries of different rotational graphene domains. (B) Magnification of graphene from the black solid square reported in (A). The honeycomb graphene lattice is modulated by a 3×3 Moiré periodicity, whose unit cell is indicated by the green solid diamond. Images parameters: (A) I = 0.2 nA, V = −1.35 V, 100×100 nm^2, scale bar = 10 nm. (B) I = 0.57 nA, V = −166 mV, 8×8 nm^2, scale bar = 2 nm. (For interpretation of the references to colour in this figure legend, the reader is referred to the web version of this article.)

radiation facility in Trieste [30] with a base pressure of ~ 5×10^{-10} mbar. XAS measurements were performed in total electron yield (TEY) mode in linear horizontal polarization, at Cr $L_{2,3}$ edges, with the sample surface at 45° with respect to the impinging beam. XPS spectra were taken with a Scienta R3000 analyzer, with the same geometry of XAS measurements, being the sample normal to the analyzer. The impinging photon energy used for XPS measurements was set to 900 eV. The valence band of a gold reference foil was used to correctly align the binding energies of all spectra. For both XAS and XPS measurements, the area probed by the beam spot was around 200×200 μm^2. All measurements were taken at room temperature.

3. Results and discussion

The LEED patterns for Cr_2O_3 ultrathin films at different thicknesses are presented in Fig. 1, for both bare Pt(1 1 1) (Fig. 1A) and Gr/Pt(1 1 1) (Fig. 1B). In the former case, the presence of a sharp (1×1) hexagonal diffraction pattern before Cr_2O_3 deposition is proof of the order and cleanliness of the substrate surface. The same starting conditions have been obtained and verified also in the case of Cr_2O_3 growth on Gr/Pt (1 1 1).

In the bare case, different surface reconstruction are obtained upon Cr_2O_3 deposition as a function of its thickness. In particular, a clear (2×2) reconstruction is identified after the deposition of 2 MLs of Cr_2O_3 (Fig. 1A). Increasing the oxide thickness up to roughly 8 MLs, the diffraction pattern changes, becoming a superposition of two structures, namely a clear ($\sqrt{3}\times\sqrt{3}$)R30° pattern and a faint (2×2) reconstruction, signature of a coexistence of two different oxide structural domains on the Pt(1 1 1) surface, in good agreement with what reported in literature for the same thicknesses [23,31].

On the other hand, once the Gr intralayer is included, the differences on the obtained diffraction pattern strongly influence the following Cr_2O_3 growth quality (Fig. 1B). Gr is known to be weakly interacting on Pt(1 1 1), and its Moiré structures and domain dimensions are strongly dependent on temperature deposition [32–34]. In this case, the LEED pattern presents arc-shaped spots on top of the preserved (1×1) hexagonal pattern of the substrate. This is indicative of the presence of a locally ordered Gr layer, composed by different domains of varying orientation. The centers of the arc-shape spots correspond to 19° and 30° of rotation, in good agreement with what reported in literature for similar Gr growth temperatures [32].

When Cr_2O_3 is grown on top of this multidomain configuration, no additional diffraction patterns, and therefore no reconstructions, are found (Fig. 1B), in contrast with the bare Pt(1 1 1) case. Instead, the intensity of the Gr and Pt spots progressively decreases after each incremental deposition. In this case, Cr_2O_3 MLs do not have evident structural order, giving no additional reconstruction. In particular, the LEED pattern of the 2 MLs Cr_2O_3/Gr/Pt clearly shows the diffraction spots of Pt and the ring associated to Gr, and even at a coverage of 8 MLs they are still visible, although weaker, suggesting that the nucleation of Cr oxide on Gr follows a Volmer-Weber scheme [35].To confirm the presence of a multidomain Gr layer, we investigate the surface in the real space via STM measurements. An example of the surface morphology is reported in Fig. 2. In the large-scale topographical image of Fig. 2A, we see a good Gr coverage over the whole probed area.

More into details, a black dashed line helps the eye to identify the borders of different domains, rotated at different angles, confirming the presence of Gr multidomains. In Fig. 2B, an atomically resolved magnification of the surface from the solid black square in the large-scale image points out the local good quality of the Gr honeycomb lattice, confirming its homogeneity in a single domain. The lattice is modulated by a 3×3 periodicity (Moiré superstructure with respect to Gr) of roughly 0.7 nm. Based on literature, this periodicity could be ascribed to a Gr domain whose rotation angle between Gr and Pt lattices is around 19° [32], in perfect agreement with the LEED patterns shown in Fig. 1B.

Once compared the structural characteristics of the two cases, we move to the electronic characterization via XPS and XAS measurements. Fig. 3 shows the XPS spectra as a function of the incremental growths for both bare Pt(1 1 1) and Gr/Pt(1 1 1). Starting from the former case, the lack of detectable Cr *2p* and O *1s* signals before Cr_2O_3 growth (black lines in Fig. 3A) further confirms the cleanliness of the surface after sputtering/annealing cycles. After 2 MLs Cr_2O_3 deposition, Cr *2p* and O *1s* peaks start rising up (blue spectra in Fig. 3A). Increasing the Cr_2O_3 thickness up to 8 MLs, the Cr *2p* and O *1s* peaks increase their intensity and sharpness (red spectra in Fig. 3A), consistently with the growth of a thicker oxide overlayer. Here, clear features can be identified: in the case of Cr *2p* edges, the two peaks are centered at 586.30 eV and 576.52 eV, respectively, in good agreement with the binding energies ascribed in literature to Cr $2p_{1/2}$ and to Cr $2p_{3/2}$ edges in the Cr_2O_3 configuration [36,37]. On the other hand, also the peak in the energy range of O *1s* increases, proportionally with the increasing Cr *2p* peak. We report a 0.4 eV shift from 530.2 eV for 2 MLs thickness to 529.8 eV at 8 MLs, usually

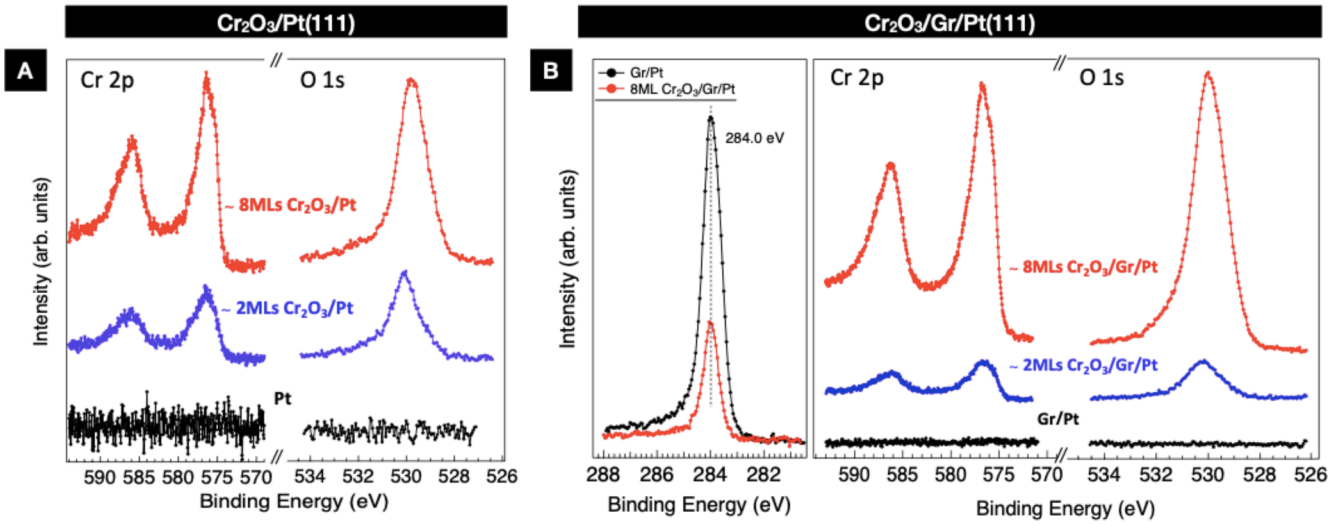

Fig. 3. Cr *2p* and O *1s* core levels spectra at different Cr_2O_3 growth steps on (A) bare Pt(1 1 1), hv = 923 eV, and on (B) Gr/Pt(1 1 1), hv = 910 eV. The XPS spectra clearly show the rising of Cr *2p* and O *1s* peaks for incremental growth of Cr_2O_3. In (B), C 1s peaks are reported for clean Gr/Pt and 8 MLs Cr_2O_3/Gr/Pt. The decreasing in intensity of the peak without a detectable shift of the BE is a strong indication of the Cr oxide growth on top of Gr, with no sign of interface intercalation or degradation of the carbon layer.

assigned to the hydroxide/adsorbed oxygen species and to the oxide form (i.e. Cr–O–Cr bonds), respectively [38,39].

Likewise the case of Cr_2O_3 grown on bare Pt (Fig. 3A), the XPS spectra of Cr_2O_3 grown on multidomain Gr/Pt, as shown for each incremental growth in Fig. 3B, appear similar.

Also in this case, we confirm the lack of Cr *2p* and O *1s* contaminants after Gr growth (black lines in Fig. 3B), while the C *1s* peak, centered at 284.0 eV, shows no sign of any spurious C contribution [40]. Well defined peaks at both the Cr *2p* and O *1s* edges are found after the deposition of 2 MLs of Cr_2O_3 (blue spectra in Fig. 3B), which become evident and sharp upon 8 MLs Cr_2O_3 deposition (red spectra in Fig. 3B).

The shape and the binding energies at which these components are centered (586.7 eV, 576.85 eV and 530.08 eV for Cr $2p_{1/2}$, Cr $2p_{3/2}$ and O *1s*, respectively) match with those we found for the case of Cr_2O_3 on bare Pt, and are consistent with what reported in literature [36–38]. This confirms the growth of a stoichiometric Cr_2O_3 from the very early stages, upon multidomain Gr/Pt(1 1 1). We also remark that the C *1s* intensity decreases after Cr_2O_3 deposition, without either changing its binding energy position or showing any peak broadening. This is a strong indication of a growth on top of the Gr/Pt system, with no signs of Gr degradation or Cr_2O_3 intercalation upon deposition. Therefore, these photoemission measurements show how ultrathin Cr_2O_3 is electronically well defined and stoichiometric not only when well structurally grown on bare Pt, but also on a more inhomogeneous interface, as in the case of multidomain Gr/Pt.

To further corroborate this result, we show the XAS spectra taken at the Cr $L_{2,3}$ edges along the same incremental growth steps for both cases. The reason of this is in the high sensitivity even in presence of very low coverages given by absorption spectra in TEY mode [42], which allows for more detailed comparisons between the two systems. Fig. 4A shows the absorption spectra related to the same Cr_2O_3 coverages previously investigated by XPS. To facilitate the analysis of the results, a Cr_2O_3 reference spectrum from Ref. [41] is added for comparison. Here, the main features of the L_3 edge, correlated to the relative strength of the atomic and crystal field interactions, are labelled [43,44]. All the measured XAS spectra, reported in Fig. 4A, show the lineshape corresponding to a pure Cr^{3+} oxidation state, consistently with the expected stoichiometry and therefore in agreement with the XPS characterization.

Both L_3 and L_2 peaks are well-defined and nicely retrace the reference ones. By carefully comparing the L_3 features in presence and in absence of the Gr intralayer and at the two thicknesses, we can estimate the electronic differences for all cases. In details, at low coverages, all features appear slightly broader, becoming sharper as the thickness of chromium oxide increases. In particular, the two main peaks A and B, at the L_3 edge, are clearly evident in all the spectra acquired at different coverages in both systems; C becomes more prominent at higher thickness, while D is not well defined in all the measured spectra. Focusing on the higher coverage case, we notice that the pre-edge A is less pronounced compared to the reference spectra, giving higher B/A ratios. A magnification of the L_3 peak for these two spectra, reported in Fig. 4B, shows that, while almost all features perfectly overlap, slight differences are present in the shape of A and C peaks. These appear to be more pronounced and closer to the reference one in the case of Cr_2O_3 on bare Pt(1 1 1). This is also confirmed by the more defined peak on bare Pt (1 1 1) at the L_2 edge, as can be seen in Fig. 4A. We attribute this to the differences in growth quality, as observed from LEED patterns in Fig. 1. While there we could notice that Cr_2O_3 had no reconstructions once grown on multidomain Gr/Pt(1 1 1), here the effects on the electronic properties are much less important, with just a slight broadening of the spectra. Our combined spectroscopic investigation shows that ultrathin Cr_2O_3 grown on multidomains Gr presents the proper stoichiometry and electronic properties, almost perfectly overlapping with those of Cr_2O_3 on bare Pt, despite the lack of long-range structural order due to the higher inhomogeneity of the Gr intralayer leading to a three-dimensional nucleation of the Cr_2O_3 growth. Nevertheless, this is encouraging in the envision of Cr_2O_3 implementation on Gr-integrated heterostructures, with the possibility of exploiting its magnetoelectric properties for spintronic applications.

4. Conclusions

By means of LEED, XPS and XAS characterizations, we have compared the electronic and structural qualities of ultrathin Cr_2O_3 films grown on bare Pt(1 1 1) and on multidomain Gr/Pt(1 1 1). In the former case, Cr_2O_3 shows high-quality long-range order from the very first MLs, with a (2×2) reconstruction at 2 MLs and a mixture of a $(\sqrt{3}\times\sqrt{3})R30°$ and a (2×2) reconstructions at 8 MLs, consistently with literature, showing sharp and well-defined XPS and XAS spectra that confirm the stoichiometry and electronic properties, in good agreement with what reported for thicker films. Once a Gr intralayer, of which LEED and STM measurements report a randomly oriented multidomain growth, is included in-between the Pt(1 1 1) substrate and Cr_2O_3 MLs, the long-

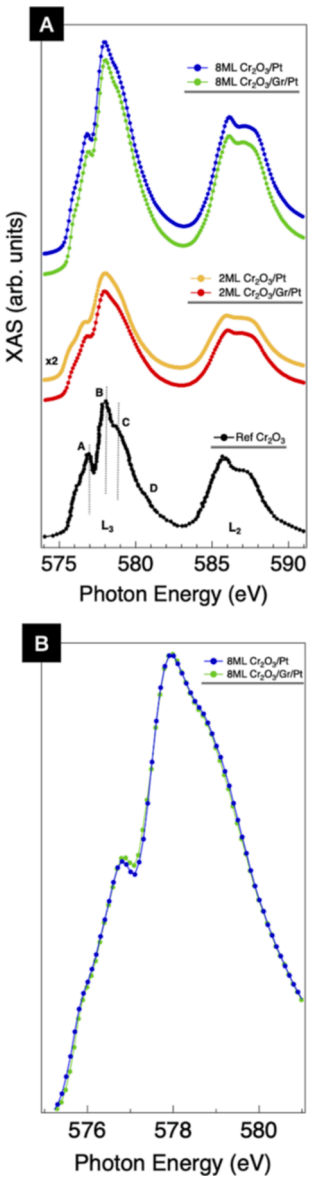

Fig. 4. (A) XAS spectra acquired at the Cr $L_{2,3}$ edges for Cr_2O_3/Pt(1 1 1) and Cr_2O_3/Gr/Pt(1 1 1). We compared different Cr oxide thicknesses: 2 MLs (orange and red curves, respectively) and 8 MLs (blue and green curves, respectively) of Cr_2O_3. Below, in black, a reference spectrum for Cr_2O_3 is shown from Ref. [41]. In both cases, similar features are observed, better defined at higher thicknesses. (B) A magnification of the L_3 peak of the two overlapped curves for 8 MLs Cr_2O_3 on bare Pt and on Gr/Pt is shown. Tiny differences are visible in correspondence to A and C peaks, where the features of Cr_2O_3/Pt(1 1 1) are better defined than those of Cr_2O_3/Gr/Pt(1 1 1). (For interpretation of the references to colour in this figure legend, the reader is referred to the web version of this article.)

range morphological order is partially lost because of the higher interfacial morphological inhomogeneity which induces the three-dimensional nucleation of the oxide. Despite that, our spectroscopic characterizations show almost no modifications in the electronic properties of the ultrathin Cr_2O_3 films compared to the structurally reconstructed case, with correct stoichiometry and well-defined spectral features. These results promote Cr_2O_3 as a promising candidate for Gr-integrated 2D heterostructures, thanks to the lack of interdiffusion and the low requirements on interfacial morphological order, and stimulate for further investigations on its correlated antiferromagnetic and magnetoelastic properties.

CRediT authorship contribution statement

Sara Fiori: Investigation, Formal analysis, Validation, Conceptualization, Writing – original draft, Visualization. **Deepak Dagur:** Investigation, Validation, Writing – review & editing. **Michele Capra:** Investigation, Validation, Writing – review & editing. **Andrea Picone:** Investigation, Validation, Writing – review & editing. **Alberto Brambilla:** Writing – review & editing, Supervision, Funding acquisition. **Piero Torelli:** Writing – review & editing, Supervision. **Giancarlo Panaccione:** Writing – review & editing, Supervision, Funding acquisition. **Giovanni Vinai:** Investigation, Validation, Conceptualization, Writing – original draft, Project administration, Supervision.

Declaration of Competing Interest

The authors declare that they have no known competing financial interests or personal relationships that could have appeared to influence the work reported in this paper.

Data availability

Data will be made available on request.

Acknowledgment

This work has been performed in the framework of the Nanoscience Foundry and Fine Analysis (NFFA- MUR Italy Progetti Internazionali) project (www.trieste.NFFA.eu) and has received funding from the European Union's Horizon 2020 Research and Innovation Programme under Project SINFONIA, Grant 964396. We thank Andrea Fondacaro and Jun Fujii for technical support and fruitful discussions.

References

[1] K.S. Novoselov, A.K. Geim, S.V. Morozov, D. Jiang, Y. Zhang, S.V. Dubonos, I. V. Grigorieva, A.A. Firsov, Electric field effect in atomically thin carbon films, Science 306 (5696) (2004) 666–669.
[2] M. Gibertini, M. Koperski, A.F. Morpurgo, K.S. Novoselov, Magnetic 2D materials and heterostructures, Nat. Nanotechnol. 14 (5) (2019) 408–419.
[3] S. Yang, C. Jiang, S. Wei, Gas sensing in 2D materials, Appl. Phys. Rev. 4 (2) (2017), 021304.
[4] B. Luo, G. Liu, L. Wang, Recent advances in 2D materials for photocatalysis, Nanoscale 8 (13) (2016) 6904–6920.
[5] X. Yan, K. Wang, J. Zhao, Z. Zhou, H. Wang, J. Wang, L. Zhang, X. Li, Z. Xiao, Q. Zhao, Y. Pei, G. Wand, C. Qin, J. Lou, Q. Liu, P. Zhou, A new memristor with 2D $Ti_3C_2T_x$ MXene flakes as an artificial Bio-Synapse, Small 15 (25) (2019) 1900107.
[6] K.S. Novoselov, O.A. Mishchenko, O.A. Carvalho, A.H. Castro Neto, 2D materials and van der Waals heterostructures, Science 353(6298) (2016) aac9439.
[7] G. Iannaccone, F. Bonaccorso, L. Colombo, G. Fiori, Quantum engineering of transistors based on 2D materials heterostructures, Nat. Nanotechnol. 13 (3) (2018) 183–191.
[8] D.V. Dimitrov, S. Zhang, J.Q. Xiao, G.C. Hadjipanayis, C. Prados, Effect of exchange interactions at antiferromagnetic/ferromagnetic interfaces on exchange bias and coercivity, Phys. Rev. B 58 (18) (1998) 12090.
[9] R. Zhu, W. Zhang, W. Shen, P.K.J. Wong, Q. Wang, Q. Liang, Z. Tian, Y. Zhai, C. Qiu, A.T.S. Wee, Exchange bias in van der Waals $CrCl_3/Fe_3GeTe_2$ heterostructures, Nano Lett. 20 (7) (2020) 5030–5035.
[10] M. Finazzi, L. Duo, F. Ciccacci, Magnetic properties of interfaces and multilayers based on thin antiferromagnetic oxide films, Surf. Sci. Rep. 64 (4) (2009) 139–167.
[11] L. Duò, M. Finazzi, F. Ciccacci, Magnetic Properties of Antiferromagnetic Oxide Materials: Surfaces, Interfaces, and Thin Films, John Wiley & Sons, 2010.
[12] S. Surnev, A. Fortunelli, F.P. Netzer, Structure–property relationship and chemical aspects of oxide–metal hybrid nanostructures, Chem. Rev. 113 (6) (2013) 4314–4372.
[13] G. Barcaro, A. Fortunelli, 2D oxides on metal materials: concepts, status, and perspectives, PCCP 21 (22) (2019) 11510–11536.
[14] A. Picone, M. Riva, A. Brambilla, A. Calloni, G. Bussetti, M. Finazzi, F. Ciccacci, L. Duo, Reactive metal–oxide interfaces: a microscopic view, Surf. Sci. Rep. 71 (1) (2016) 32–76.
[15] B.M. Weckhuysenand, R.A. Schoonheydt, Alkane dehydrogenation over supported chromium oxide catalysts, Catal. Today 51 (2) (1999) 223–232.
[16] J.H. Uhm, M.Y. Shin, J. Zhidong, J.S. Chung, Selective oxidation of H_2S to elemental sulfur over chromium oxide catalysts, Appl Catal B 22 (4) (1999) 293–303.
[17] T.G. Worlton, R.M. Brugger, R.B. Bennion, Pressure dependence of the Néel temperature of Cr_2O_3, J. Phys. Chem. Solid 29 (3) (1968) 435–438.

[18] S. Mu, A.L. Wysocki, K.D. Belashchenko, Effect of substitutional doping on the Néel temperature of Cr_2O_3, Phys. Rev. B 87 (5) (2013), 054435.
[19] R. Schlitz, T. Kosub, A. Thomas, S. Fabretti, K. Nielsch, D. Makarov, S.T. B. Goennenwein, Evolution of the spin hall magnetoresistance in Cr_2O_3/Pt bilayers close to the Néel temperature, Appl. Phys. Lett. 112 (13) (2018), 132401.
[20] T. Jungwirth, X. Marti, P. Wadley, J. Wunderlich, Antiferromagnetic spintronics, Nat. Nanotechnol. 11 (3) (2016) 231–241.
[21] T. Iino, T. Moriyama, H. Iwaki, H. Aono, Y. Shiratsuchi, T. Ono, Resistive detection of the Néel temperature of Cr_2O_3 thin films, Appl. Phys. Lett. 114 (2) (2019), 022402.
[22] S.P. Pati, N. Shimomura, T. Nozaki, T. Shibata, M. Sahashi, Néel temperature of Cr_2O_3 in Cr_2O_3/Co exchange-coupled system: effect of buffer layer, J. Appl. Phys. 117 (17) (2015) 17D137.
[23] L. Zhang, M. Kuhn, U. Diebold, Epitaxial growth of ultrathin films of chromium and its oxides on Pt (111), J. Vac. Sci. Technol. A 15 (3) (1997) 1576–1580.
[24] C. Xu, M. Hassel, H. Kuhlenbeck, H.-J. Freund, Adsorption and reaction on oxide surfaces: NO, NO_2 on Cr_2O_3 (111)/Cr (110), Surf. Sci. 258 (1–3) (1991) 23–34.
[25] A. Lodesani, A. Picone, A. Brambilla, D. Giannotti, M.S. Jagadeesh, A. Calloni, G. Bussetti, G. Berti, M. Zani, M. Finazzi, L. Duó, F. Ciccacci, Graphene as an ideal buffer layer for the growth of high-quality ultrathin Cr_2O_3 layers on Ni (111), ACS nano 13 (4) (2019) 4361–4367.
[26] X. Hou, M. Wumiti, S. Kumar, K. Shimada, M. Sawada, Observation of mid-gap states emerging in the O-terminated interface of Cr_2O_3/graphene: a combined study of ab initio prediction and photoemission analysis, Appl. Surf. Sci. 594 (2022), 153416.
[27] A. Dahal, M. Batzill, Graphene–nickel interfaces: a review, Nanoscale 6 (5) (2014) 2548–2562.
[28] I.I. Klimovskikh, M.M. Otrokov, V.Y. Voroshnin, D. Sostina, L. Petaccia, G. Di Santo, S. Thakur, E.V. Chulkov, A.M. Shikin, Spin–orbit coupling induced gap in graphene on Pt(111) with intercalated Pb monolayer, ACS Nano 11 (1) (2017) 368–374.
[29] D. Nečas, P. Klapetek, Gwyddion: an open-source software for SPM data analysis, Open Phys. 10 (1) (2012) 181–188.
[30] G. Panaccione, I. Vobornik, J. Fujii, D. Krizmancic, E. Annese, L. Giovanelli, F. Maccherozzi, F. Sal-vador, A. De Luisa, D. Benedetti, A. Gruden, P. Bertoch, F. Polack, D. Cocco, G. Sostero, B. Diviacco, M. Hochstrasser, U. Maier, D. Pescia, C.H. Back, T. Greber, J. Osterwalder, M. Galaktionov, M. San-crotti, G. Rossi, Advanced photoelectric effect experiment beamline at Elettra: a surface science laboratory coupled with Synchrotron Radiation, Rev. Sci. Instrum. 80 (4) (2009), 043105.
[31] L. Zhang, M. Kuhn, U. Diebold, Growth, structure and thermal properties of chromium oxide films on Pt (111), Surf. Sci. 375 (1) (1997) 1–12.
[32] M. Gao, Y. Pan, L. Huang, H. Hu, L.Z. Zhang, H.M. Guo, S.X. Du, H.-J. Gao, Epitaxial growth and structural property of graphene on Pt (111), Appl. Phys. Lett. 98 (3) (2011), 033101.
[33] P. Sutter, J.T. Sadowski, E. Sutter, Graphene on Pt(111): growth and substrate interaction, Phys. Rev. B 80 (24) (2009), 245411.
[34] I.I. Klimovskikh, S.S. Tsirkin, A.G. Rybkin, A.A. Rybkina, M.V. Filianina, E. V. Zhizhin, E.V. Chulkov, A.M. Shikin, Nontrivial spin structure of graphene on Pt (111) at the Fermi level due to spin-dependent hybridization, Phys. Rev. B 90 (23) (2014), 235431.
[35] J.A. Floro, S.J. Hearne, J.A. Hunter, P. Kotula, E. Chason, S.C. Seel, C.V. Thompson, The dynamic competition between stress generation and relaxation mechanisms during coalescence of Volmer-Weber thin films, J. Appl. Phys. 89 (9) (2001) 4886–4897.
[36] G.P. Haladaand, C.R. Clayton, Photoreduction of hexavalent chromium during X-ray photoelectron spectroscopy analysis of electrochemical and thermal films, J. Electrochem. Soc. 138 (10) (1991) 2921.
[37] M.C. Biesinger, C. Brown, J.R. Mycroft, R.D. Davidson, N.S. McIntyre, X-ray photoelectron spectroscopy studies of chromium compounds. Surface and interface analysis: an international journal devoted to the development and application of techniques for the analysis of surfaces, Interf. Thin Films 36 (12) (2004) 1550–1563.
[38] M.F. Al-Kuhaili, S.M.A. Durrani, Optical properties of chromium oxide thin films deposited by electron-beam evaporation, Opt. Mater. 29 (6) (2007) 709–713.
[39] G.R.S.K. Hollinger, R. Skheyta-Kabbani, M. Gendry, Oxides on GaAs and InAs surfaces: an x-ray-photoelectron-spectroscopy study of reference compounds and thin oxide layers, Phys. Rev. B 49 (16) (1994) 11159.
[40] A.B. Preobrajenski, M.L. Ng, A.S. Vinogradov, N. Mårtensson, Controlling graphene corrugation on lattice-mismatched substrates, Phys. Rev. B 78 (7) (2008), 073401.
[41] G.C. Vásquez, D. Maestre, A. Cremades, J. Ramírez-Castellanos, E. Magnano, S. Nappini, S.Z. Karazhanov, Understanding the effects of Cr doping in rutile TiO_2 by DFT calculations and X-ray spectroscopy, Sci. Rep. 8 (1) (2018) 1–12.
[42] N. Giaconi, A.L. Sorrentino, L. Poggini, M. Lupi, V. Polewczyk, G. Vinai, P. Torelli, A. Magnani, R. Sessoli, S. Menichetti, L. Sorace, C. Viglianisi, M. Mannini, Stabilization of an enantiopure submonolayer of helicene radical cations on a Au (111) surface through noncovalent interactions, Angew. Chem. Int. Ed. 60 (28) (2021) 15276–15280.
[43] Y.S. Dedkov, A.S. Vinogradov, M. Fonin, C. König, D.V. Vyalikh, A. B. Preobrajenski, S.A. Krasnikov, E.Y. Kleimenov, M.A. Nesterov, U. Rüdiger, S. L. Molodtsov, G. Güntherodt, Correlations in the electronic structure of half-metallic ferromagnetic CrO_2 films: an x-ray absorption and resonant photoemission spectroscopy study, Phys. Rev. B 72 (6) (2005), 060401.
[44] C. Theil, J. Van Elp, F. Folkmann, Ligand field parameters obtained from and chemical shifts observed at the Cr $L_{2,3}$ edges, Phys. Rev. B 59 (12) (1999) 7931.